AGU PUBLICATIONS

JGR

Journal of Geophysical Research: Solid Earth

RESEARCH ARTICLE

10.1002/2017JB015182

Key Points:
- Calbuco 2015 eruption observed in local seismic (<15 km), regional seismo-acoustic (15–250 km), and remote acoustic data (>250 km) to 5,122 km
- Remote infrasound arrays provide accurate explosion chronology consistent with regional and local data and permit automated source location
- Regional seismo-acoustic networks augment the International Monitoring System and enhance volcanic signal detection

Supporting Information:
- Supporting Information S1
- Movie S1
- Movie S2

Correspondence to:
R. S. Matoza,
rmatoza@ucsb.edu

Citation:
Matoza, R. S., Fee, D., Green, D. N., Le Pichon, A., Vergoz, J., Haney, M. M., et al. (2018). Local, regional, and remote seismo-acoustic observations of the April 2015 VEI 4 eruption of Calbuco volcano, Chile. *Journal of Geophysical Research: Solid Earth*, *123*, 3814–3827. https://doi.org/10.1002/2017JB015182

Received 2 NOV 2017
Accepted 3 MAR 2018
Accepted article online 7 MAR 2018
Published online 8 MAY 2018

Local, Regional, and Remote Seismo-acoustic Observations of the April 2015 VEI 4 Eruption of Calbuco Volcano, Chile

Robin S. Matoza[1], David Fee[2], David N. Green[3], Alexis Le Pichon[4], Julien Vergoz[4], Matthew M. Haney[5], T. Dylan Mikesell[6], Luis Franco[7], O. Alberto Valderrama[7], Megan R. Kelley[1,8], Kathleen McKee[2], and Lars Ceranna[9]

[1]Department of Earth Science and Earth Research Institute, University of California, Santa Barbara, Santa Barbara, CA, USA, [2]Wilson Alaska Technical Center, Alaska Volcano Observatory, Geophysical Institute, University of Alaska Fairbanks, Fairbanks, AK, USA, [3]AWE Blacknest, Reading, UK, [4]CEA, DAM, DIF, Arpajon, France, [5]Alaska Volcano Observatory, U.S. Geological Survey Volcano Science Center, Anchorage, AK, USA, [6]Department of Geosciences, Boise State University, Boise, ID, USA, [7]Observatorio Volcanológico de los Andes del Sur, Servicio Nacional de Geología y Minería, Temuco, Chile, [8]Now at Department of Earth and Planetary Sciences, University of California, Santa Cruz, CA, USA, [9]BGR, Hannover, Germany

Abstract The two major explosive phases of the 22–23 April 2015 eruption of Calbuco volcano, Chile, produced powerful seismicity and infrasound. The eruption was recorded on seismo-acoustic stations out to 1,540 km and on five stations (IS02, IS08, IS09, IS27, and IS49) of the International Monitoring System (IMS) infrasound network at distances from 1,525 to 5,122 km. The remote IMS infrasound stations provide an accurate explosion chronology consistent with the regional and local seismo-acoustic data and with previous studies of lightning and plume observations. We use the IMS network to detect and locate the eruption signals using a brute-force, grid-search, cross-bearings approach. After incorporating azimuth deviation corrections from stratospheric crosswinds using 3-D ray tracing, the estimated source location is 172 km from true. This case study highlights the significant capability of the IMS infrasound network to provide automated detection, characterization, and timing estimates of global explosive volcanic activity. Augmenting the IMS with regional seismo-acoustic networks will dramatically enhance volcanic signal detection, reduce latency, and improve discrimination capability.

1. Introduction

Calbuco volcano, Chile (41.3300°S, 72.6183°W), erupted explosively in April 2015 in two subplinian phases (plume heights >15 km, VEI 4) following relatively modest precursory activity (Castruccio et al., 2016; Romero et al., 2016; Valderrama et al., 2015, 2016; Van Eaton et al., 2016). A minor increase in volcano-tectonic (VT) events (local magnitudes <2, ~5 events per day) was detected on local and regional seismic stations in the 3 months preceding the eruption (i.e., from February 2015); these events were located between the crater of the volcano and 6 km to the west, with depths of 5–9 km (Valderrama et al., 2015). We nominally define recording distances as local: <15 km, regional: 15–250 km, and remote: >250 km (Fee & Matoza, 2013). A significant, rapid, escalation in shallow seismicity (VT and long-period, LP, including events classified by Observatorio Volcanológico de los Andes del Sur (OVDAS) as "hybrid" based on frequency content and waveform) occurred in the 3–4 h prior to the first explosive phase (Figure 1) (Castruccio et al., 2016; Valderrama et al., 2016, 2015). This preeruptive seismicity sequence included a local magnitude M_L 3.8 event located to the west of Calbuco at 6.3 km depth (OVDAS solution), approximately ~20 min before the eruption (Figure 1) (Valderrama et al., 2015, 2016). Van Eaton et al. (2016) provide a chronology of the eruption combining data from a local seismic station (station PES ~5.4 km distance from the crater), satellite-derived umbrella cloud expansion estimates, lightning mapping, and characteristics of the fall deposits. The two major subplinian explosive phases are estimated to have begun at 21:04 22 April 2015 (duration ~1 h:30 m) and 04:00 23 April 2015 (duration ~6 h:15 m) (Van Eaton et al., 2016) (we report all times in UT and all plume heights referenced to above sea level). These explosive phases were characterized by ash columns extending into the stratosphere, with a maximum plume height of 23 km (Vidal et al., 2015) and pyroclastic density currents reaching 6 km from the vent (Castruccio et al., 2016). These events resulted in the evacuation of over 6,500 people from nearby communities and impacted infrastructure, agriculture, and aviation. The two major eruptive phases were also detected using ionospheric total electron content perturbations on ground-based Global Navigation Satellite System receivers in southern Chile, interpreted as a consequence of acoustic

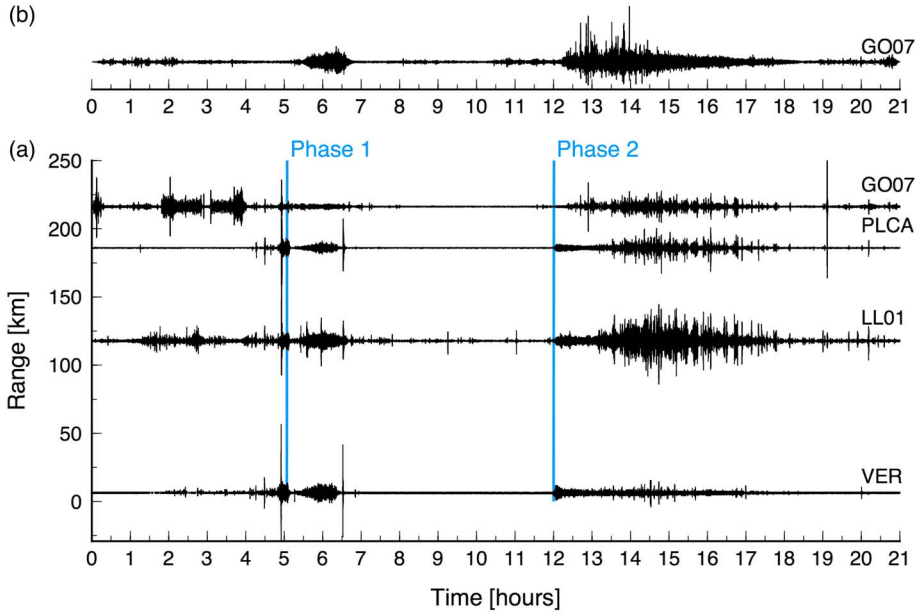

Figure 1. (a) Record section of broadband seismic data (vertical component, band-pass filtered 0.5–10 Hz, except VER unfiltered) showing the precursory seismicity and two explosive phases of Calbuco. Station distances to Calbuco are VER (6.3 km), LL01 (118 km), PLCA (186 km), and GO07 (216 km). The plot origin time is 16:00 22 April 2015. The eruption start times (Van Eaton et al., 2016) are shown as blue lines with a moveout velocity of 6.8 km/s. Station GO07 is a colocated seismo-acoustic station; (b) its infrasound data band-pass filtered 0.1–18 Hz. Note the asymmetric, positively skewed infrasound waveforms during hours 12 to 15. Also note the strong similarity between PLCA and GO07 seismic data from 15 to 17 h.

shocks that propagated to ionospheric altitudes (Shults et al., 2016). A third smaller (likely phreatic) explosive eruption occurred at 16:08 30 April 2015 (plume height $<$4.5 km) (Van Eaton et al., 2016); the third event did not produce large enough signals to be recorded beyond local distances. Here we focus on using remote infrasound signals to locate and characterize the two major explosive eruption events on 22–23 April 2015.

Previous work has demonstrated that remote infrasound arrays can be used to detect, locate, and provide detailed chronologies of remote explosive volcanism, with the potential to provide source parameters for ash transport and dispersal models (e.g., Caudron et al., 2015; Dabrowa et al., 2011; Fee, Steffke, & Garces, 2010; Green et al., 2013; Matoza, Le Pichon, et al., 2011; Matoza, Vergoz, et al., 2011). Regional volcano-acoustic monitoring and early warning systems are being investigated and implemented (De Angelis et al., 2012; Garces et al., 2008; Fee, Garces, & Steffke, 2010; Kamo et al., 1994; Matoza et al., 2007; Ulivieri et al., 2013). More recent work has explored the potential of the International Monitoring System (IMS) infrasound network to provide a quantitative catalog of global explosive volcanic activity (Matoza et al., 2017) and automated eruption notifications to Volcanic Ash Advisory Centers (Mialle et al., 2015). The well-documented 22–23 April 2015 eruptive sequence of Calbuco represents a unique opportunity to test and evaluate remote infrasonic detection, location, and characterization capabilities. We evaluate the ability of remote IMS infrasound stations to (1) detect volcanic eruption signals in the presence of wind noise and interfering infrasound signals, (2) provide fast and reliable location solutions using automated procedures, and (3) provide constraints on the timing (origin time and duration) of explosive eruptive activity. The availability of local seismic, regional seismo-acoustic, and remote acoustic data makes this a useful case study for this purpose. In addition, the April 2015 eruption of Calbuco represents a rare case of a large ground-truth infrasound event in the Southern Hemisphere. Very few ground-truth infrasound events have been available for the Southern Hemisphere to date, due in part to the lower station density and correspondingly lower detection capability (Le Pichon et al., 2009) and due to the reduced number of anthropogenic sources in the more sparsely populated hemisphere (Nippress & Green, 2017). Furthermore, Earth's potentially active volcanoes are unevenly distributed by hemisphere, with only about 19% located between 10° south and the South Pole (Global Volcanism Program, 2013).

2. Regional and Remote Infrasound Observations

The IMS includes a global network of infrasound arrays designed to detect atmospheric explosions anywhere on the planet (Figure 2); 60 stations are planned with an average spacing of about 2,000 km and 49 stations are currently certified (Christie & Campus, 2010). Each infrasound station is an array of at least four infrasonic sensors that digitally sample atmospheric pressure at 20 Hz. The sensors have a flat response compliant with IMS minimum requirements from 0.02 to 4 Hz and a sensitivity of about 0.1 mPa per count. Five IMS stations (IS02, IS08, IS09, IS27, and IS49) detected the April 2015 Calbuco eruption (Figures 2 and 3). A detection is defined here as a coherent array detection sequence using the Progressive Multichannel Correlation (PMCC) method (Le Pichon et al., 2010) that arrives at the appropriate time and backazimuth, and which we can confidently discriminate from persistent background coherent infrasound signals (clutter) (Matoza et al., 2013). IS02 (1,525 km), IS08 (2,809 km), and IS09 (3,698 km) recorded both subplinian explosive phases. Due to varying noise levels (Figure 4), IS27 (4,800 km) detected only Phase 2 and IS49 (5,122 km) detected only Phase 1. Only one channel (H2) of IS41 was functioning during this time, which did clearly record both explosive phases (Figure 4); however, array processing and detection were consequently not possible for this station. The meteorological conditions at station IS27 resulted in high wind-noise levels during the eruption, with wind speeds well above 10 m/s starting on 22 April 2015 in the late afternoon and persisting for at least 3 days. Wind noise levels are usually high at station IS49 given its island location in the Atlantic Ocean.

Analysis of the IMS data from Calbuco reinforces the utility of arrays for the detection of remote volcanic infrasound and its discrimination from incoherent wind noise (Walker & Hedlin, 2010) and clutter (Matoza et al., 2013) (Figures 3 and 4). For example, the predicted arrival time of Phase 1 on IS27 roughly coincides with a broadband, long-duration pressure fluctuation superficially resembling volcanic jetting (Matoza et al., 2009); however, array processing identifies this to be incoherent wind noise (Figure 4). Furthermore, the closest station IS14 (Robinson Crusoe Island, Chile; 1,011 km) registers coherent signals at the right time coming from the same backazimuth as Calbuco, which we identify as clutter, possibly surf (Garcés et al., 2003; Le Pichon et al., 2004; Matoza et al., 2013) based on a longer time series of array detections (not shown).

The April 2015 Calbuco eruption signals were also well recorded by local and regional seismic and infrasound stations (Figures 1, 3, and 4). Our analysis includes one local broadband seismic station (VER) operated by OVDAS (the OVDAS preeruptive monitoring network consisted of four seismic stations and one camera; at the time of writing the network now consists of three seismic stations, one infrasound station, and one tiltmeter) and additional regional data publicly available through the Incorporated Research Institutions for Seismology Data Management Center (IRIS DMC). In particular, the Chilean seismic network operates 10 seismo-acoustic stations, each consisting of a three-component broadband seismometer colocated with a single infrasound sensor, which provide a valuable complement to the global IMS data (IRIS DMC, 2012; http://ds.iris.edu/spud/infrasoundevent/12678628).

Infrasound is recorded above noise on four regional stations out to 1,540 km (GO07, GO08, GO04, and GO03). Only one station (GO07, 216 km) recorded both infrasound and seismic signals from Calbuco (Figure 1), permitting seismo-acoustic sensor pair analysis (Ichihara et al., 2012; Matoza & Fee, 2014). The infrasound waveform at GO07 contains portions with asymmetric, positively skewed waveforms (Figure 1), similar to previous observations 264 km from the eruption of Nabro volcano, Eritrea that were attributed to a source process linked to supersonic flow of a volcanic jet (section 4) (Fee et al., 2013). Although this was interpreted by Fee et al. (2013) as a source effect, it remains possible for the Nabro case that this is partially or entirely a propagation effect resulting from nonlinear reshocking at thermospheric altitudes (Lonzaga et al., 2015).

Seismic signals associated with the Calbuco eruption are recorded out to ~250 km on stations VER, LL01, PLCA, and GO07 (Figures 1 and 2), consisting of a combination of impulsive volcanic earthquake signals, sustained seismic eruption tremor, and air-ground coupled infrasound. Another local broadband OVDAS station, PES, shows similar waveforms to those shown in Figure 1 for VER but with some telemetry gaps (Van Eaton et al., 2016). Discrete seismic events show clear *P* and *S* phases propagating with moveouts of 6.8 km/s and 3.8 km/s, respectively, presumably representing bulk averages of crustal V_p and V_s in the region. The precursory seismicity observed locally at VER (and PES) was partially recorded at PLCA but is obscured by noise at LL01 and GO07 (Figure 1).

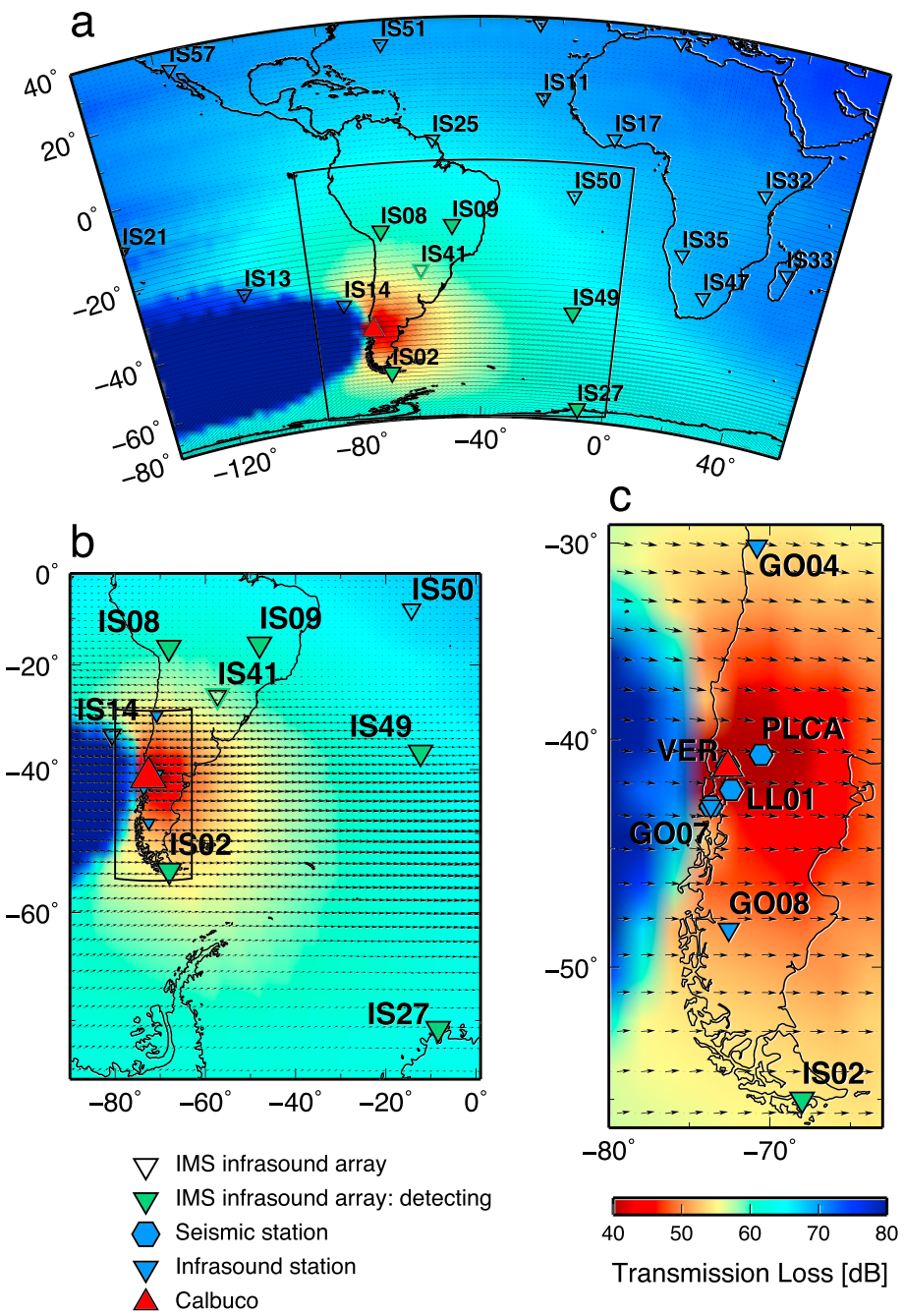

Figure 2. Map showing Calbuco (red triangle), certified stations of the IMS network (empty inverted triangles), detecting IMS stations (green inverted triangles), regional infrasound stations (blue inverted triangles), and regional seismic stations (blue hexagons). Black arrows indicate the direction and relative strength of the ECMWF stratospheric wind field averaged between elevations from 40 to 60 km. The colored grid displays the predicted transmission loss in decibels (dB) relative to a reference distance 1 km from the source at 0.5 Hz using the ECMWF wind field and the method of Le Pichon et al. (2012). Only one channel of IS41 was functioning during this time, which did record the eruption (see Figure 4). IMS = International Monitoring System; ECMWF = European Centre for Medium-Range Weather Forecasting.

The regional seismo-acoustic data provide valuable information on the eruption that is consistent with other observations. Infrasound-derived eruption origin times for the two main phases, assuming a celerity of 0.3 km/s, are 21:04 22 April 2015 and 04:00 23 April 2015, respectively (Figure 3 and Tables 1a and 1b). These origin times are consistent with those derived with local seismic data (21:04 22 April 2015; 03:54 23 April 2015) (Figure 1) and lightning analysis (21:04 22 April 2015; 04:00 23 April 2015) (Van Eaton et al., 2016). The eruption end times are also consistent within a few minutes. Both eruption phases begin

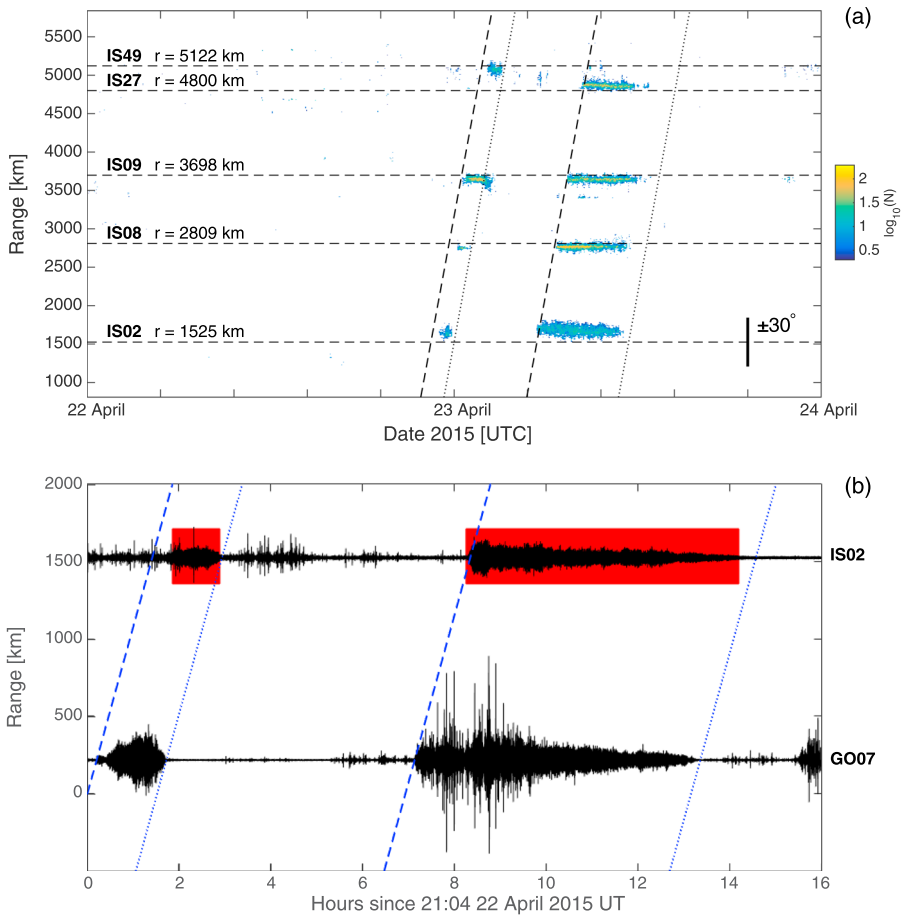

Figure 3. Record sections of infrasonic signals from two explosive phases of Calbuco: 21:04 22 April 2015 (duration 1 h:31 m) and 04:00 23 April 2015 (duration 6 h:14 m). In both cases, diagonal dashed and dotted lines correspond to the start and end times of the explosive phases, respectively, according to Van Eaton et al. (2016) and assume a stratospheric propagation celerity of 0.3 km/s. (a) Azimuth deviation record section of IMS infrasound PMCC array detections. Observed backazimuth deviations within ±30° of the true great-circle path are scaled according to the bar in the lower right and displayed centered on the station distance from Calbuco (dashed horizontal line). Color scale corresponds to $\log_{10}(N)$ where N is the number of PMCC pixels in a bin of size 0.5° in azimuth and 3.5 min in time. (b) Waveforms filtered 0.5–9 Hz from the closest regional infrasound single-channel station GO07 (216 km) and the closest IMS array IS02 (1,525 km). IMS infrasound stations are sampled at 20 Hz; the 0.5–9 Hz filter is chosen here to show waveforms at GO07 and IS02 with the same band pass. The IS02 waveform is a time-domain beam at the observed backazimuth and trace-velocity, and the red box indicates the time of coherent PMCC array detection. IMS = International Monitoring System; PMCC = Progressive Multichannel Correlation.

emergently in the regional infrasound waveforms and gradually build in amplitude over a few hours, in agreement with the steadily increasing umbrella cloud growth (and mass eruption rate, MER) (Van Eaton et al., 2016). Lightning, pyroclastic density current (PDC) generation, and mass eruption rate were all highest in Phase 2 (Van Eaton et al., 2016). Infrasound amplitudes for Phase 2 are also higher (Figures 1 and 3b). Amplitude variations in the Phase 2 infrasound between ~05:30 and 06:30 23 April 2015 are possibly related to intermittent PDC generation (Van Eaton et al., 2016).

In order to understand the regional seismo-acoustic data, it is helpful to identify air-to-ground coupling in seismic recordings. For the Calbuco eruption, we observe differences in the polarization of the regional seismic eruption tremor signals that help to identify the recorded wave type (Figure 5). Below 2 Hz, transverse signal amplitudes are approximately 25% larger than vertical and radial components (indicating a dominant *SH* wave or Love wave L_g component). In contrast, above 2 Hz, the vertical and radial components are approximately 10% larger than the transverse (suggesting that *P*, Rayleigh waves, R_g, or air-ground coupled waves are the major component of the wavefield). Observations that the radial components of discrete earthquake and explosion signals dominate across a broad frequency band suggest that the frequency variation of the tremor wavefield is not simply a site effect (e.g., Figure 5c). This observation is consistent with air-ground coupled energy on the seismometers at higher frequencies (>2 Hz), in which elliptically polarized seismic

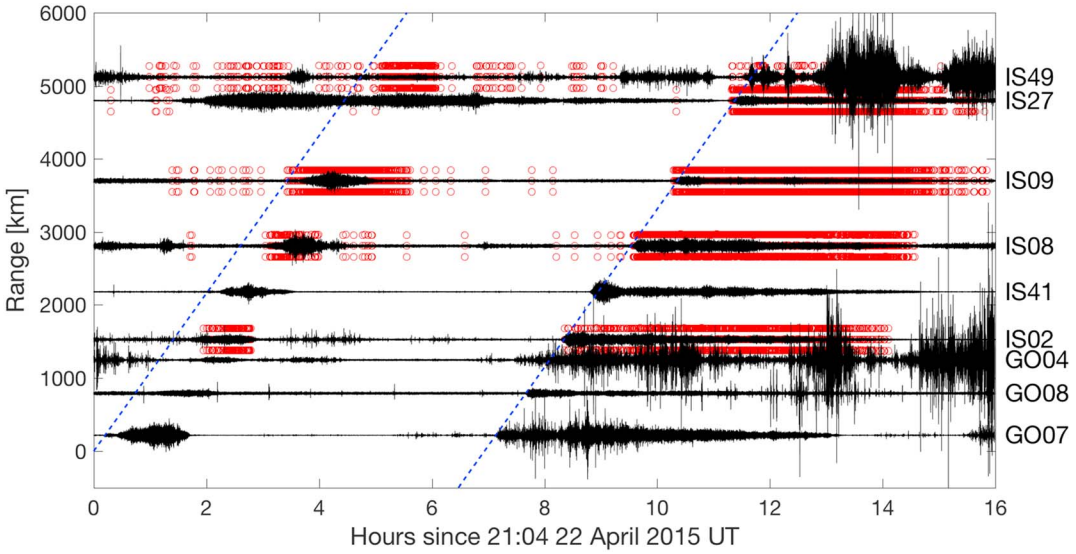

Figure 4. Record sections of infrasonic signals from the two explosive phases of Calbuco. Waveforms are normalized and represent beams in the direction of Calbuco for the IMS arrays (except IS41). Diagonal dashed lines correspond to the start times of the explosive phases (21:04 22 April 2015 and 04:00 23 April 2015), according to Van Eaton et al. (2016) and assume a stratospheric propagation celerity of 0.3 km/s. The red circles underlying the IMS infrasound array data delineate the timing of coherent PMCC detections from the direction of Calbuco (±15° of great circle path); for visibility, three red circles are plotted for each PMCC detection, with arbitrary offsets below, inline with, and above the waveform. Only one channel (H2) of IMS array IS41 was functioning during this time; the H2 waveform is shown and clearly records both explosive phases, but array processing is not possible for this station. PMCC = Progressive Multichannel Correlation; IMS = International Monitoring System.

waves are generated within the plane of propagation (Edwards et al., 2007; Ichihara et al., 2012). These air-ground coupled waves are formally guided waves and likely have a short range from the conversion point (i.e., they do not propagate coherently over kilometers, only locally near the stations) (Strick & Ginzbarg, 1956). On the one seismic station that is colocated with infrasound (GO07), cross-correlation and coherence analysis provide a strong indication of air-ground coupling (Figure 6). In addition, local seismic waveforms high-pass filtered above 5 Hz mimic long-range infrasound waveforms corrected for propagation delay, suggesting that air-ground coupling is a significant component of seismically observed eruption tremor even at local distances (Matoza & Fee, 2014).

In order to compare available constraints on eruption timing and duration, Table 1a summarizes observations from the closest recording infrasound station (GO07) and the closest recording IMS infrasound station (IS02). We estimate signal onset and duration times for both explosive phases at the stations using two methods: (1) by manual examination of the waveforms and (2) using seismo-acoustic sensor pair analysis (GO07) or PMCC (IS02). The waveforms from both explosive phases at both stations start and end gradually; our manual analysis (1) represents approximate times based on when waveforms appear and disappear below the noise level. For the seismo-acoustic sensor pair analysis (GO07), we manually measure onset and duration from the cross-correlation (XCOR) pattern (Ichihara et al., 2012). Seismo-acoustic cross-correlation relies on a signal

Table 1a
Summary of Infrasound Observations at GO07 and IS02

Station	Waveform first break	Waveform duration (s)	XCOR or PMCC onset	XCOR or PMCC duration (s)
Phase 1				
GO07 (216 km)	2015-04-22 21:16:15	5,430	2015-04-22 21:20:15	5,190
IS02 (1,525 km)	2015-04-22 22:46:40	4,600	2015-04-22 23:00:55	3,040
Phase 2				
GO07 (216 km)	2015-04-23 04:12:20	22,360	2015-04-23 04:12:20	21,280
IS02 (1,525 km)	2015-04-23 05:21:40	22,700	2015-04-23 05:25:40	20,680

Note. All times in UT. Dates are formatted as year-month-day.

Table 1b
GO07 Best (Waveform) Inferred Eruption Timing Assuming 0.3 km/s Celerity

Phase	Eruption start	Eruption duration (min)
Phase 1	2015-04-22 21:04:15	90.4
Phase 2	2015-04-23 04:00:20	372.6

Note. All times in UT. Dates are formatted as year-month-day.

on the seismometer, while PMCC has a detection threshold based on waveform correlation; thus, the XCOR- and PMCC-derived durations are shorter than those based on visible waveforms. Therefore, we judge that the manual waveform analysis of GO07 infrasound provides the most accurate timing estimates available. The relative arrival times for Phase 2 onsets at both stations are consistent with a celerity of 0.3 km/s. Based on this, Table 1b shows our best estimate for the start time and duration of both explosive phases. The inferred timings and durations from IS02 are similar to those derived from GO07 (Table 1a), confirming that remote IMS infrasound observations can provide useful constraints on the eruption timing and duration. However, the remote infrasound estimates of timing and duration contain errors of up to tens of minutes due to the emergent nature of the signals, varying wind-noise levels, and signal-to-noise ratios (Figure 4). Variations in celerity as a function of azimuth and range due to multipathing will introduce additional uncertainties in estimated eruption start time and duration, which we do not consider in this study.

3. Source Location Using Remote Infrasound Arrays

The April 2015 Calbuco eruption is a useful case study to test and validate remote infrasound signal association and source location methodologies using the IMS network. We apply the method of Matoza et al. (2017) to detect and locate the eruption signals using a brute-force, grid-search, cross-bearings approach (Figure 7). The method involves determining locations on the Earth's surface where a maximal number of signal backazimuth great-circle trajectories from multiple arrays intersect. The method described by Matoza et al. (2017) is a first-order simplified approach that does not include corrections for infrasound propagation. However, it is well known that stratospheric crosswinds (winds perpendicular to the propagation direction) result in significant azimuth deviations that translate the source location solutions (e.g., Evers & Haak, 2005; Matoza, Le Pichon, et al., 2011), as is observed in Figure 3. Observed azimuth deviations from the true great circle path (mode of the observed minus true) are IS02 (+10.8°), IS08 (−4.5°), IS09 (−5.1°), IS27 (+6.7°), and IS49 (−3.0°).

We apply the combined signal association and source-location procedure with and without a crosswind correction (Figure 7). The grids shown in Figure 7 are constructed from all signals from the five IMS arrays during the time from 22 to 23 April 2015 and have been corrected for a background prior rate of clutter predicted from the previous 10 days (Matoza et al., 2017). We apply a static azimuth deviation correction to all array detections within ±30° of the true source location. Static azimuth corrections are derived using 3-D ray tracing with the WASP-3D program (Dessa et al., 2005; Virieux et al., 2004) and the ECMWF (European Centre for Medium-Range Weather Forecasting, part of the Integrated Forecast System cycle 38r1, http://www.ecmwf.int/)

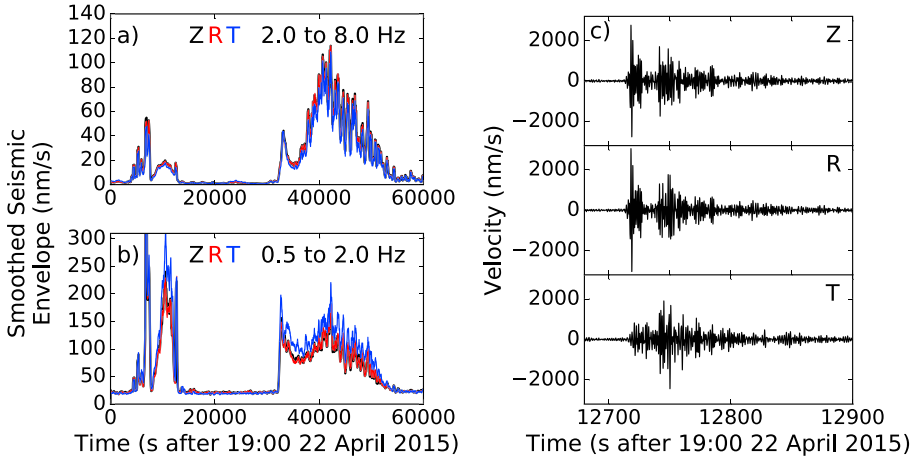

Figure 5. The seismic polarization of regional eruption tremor signals from Calbuco at station PLCA, as indicated by the relative amplitudes of vertical (*Z*), radial (*R*), and transverse (*T*) components of motion. The partitioning of seismic energy in the (a) 2.0 to 8.0 Hz and (b) 0.5 to 2.0 Hz passbands, respectively. The data are shown as the envelopes of the three components, with the envelopes smoothed using a 5 min running average window. Note the larger transverse component in the lower frequency band for the tremor signals. (c) The energy partitioning for a discrete event, presumed to be a large explosion, in the 0.5 to 2.0 Hz passband. Note that for the initial *P* wave, the transverse component amplitude is significantly smaller than the vertical and radial motions.

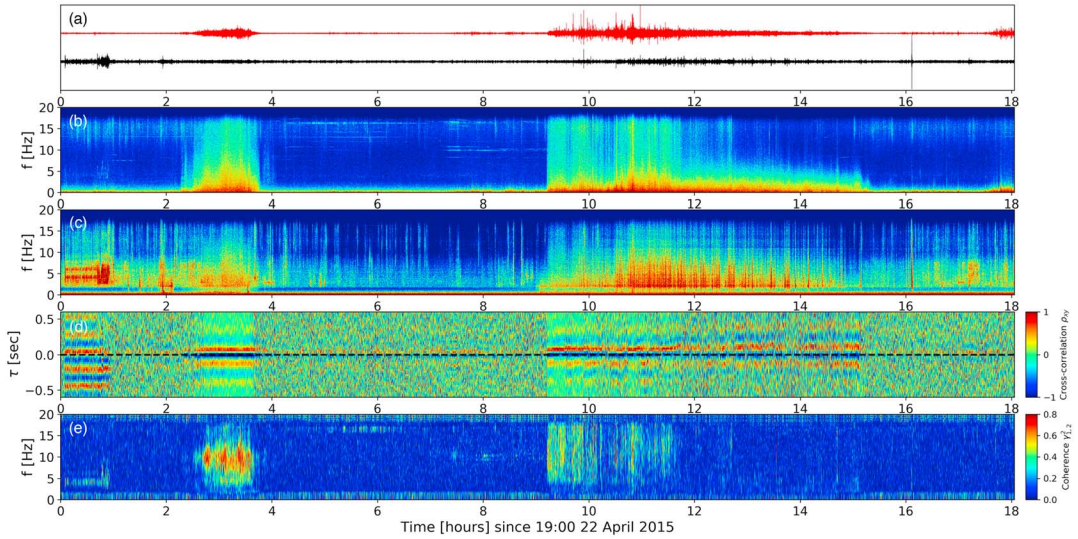

Figure 6. Seismo-acoustic cross-correlation and coherence analysis for station GO07. (a) Infrasound (red) and vertical seismic (black) waveforms filtered 3–13 Hz, (b) infrasound spectrogram, (c) vertical seismic spectrogram, (d) cross-correlation, and (e) coherence. The cross-correlation is performed with waveforms filtered 3–13 Hz, chosen based on the coherence spectrogram. Cross-correlation and coherence are performed in sliding time windows of 10 s. An unknown noise source (likely local and anthropogenic) with fixed spectral peaks from 0 to 1 h (Figure 6c) generates a similar cross-correlation signature to the eruption signals (Figure 6d).

specifications averaged over 22–23 April 2015. We note that this procedure requires the source location to be known a priori. We aim in future work to modify this approach for implementation as a blind search by computing rays from every trial source node to every receiver; however, the method used here provides an indication of the results that could be achieved with such a method.

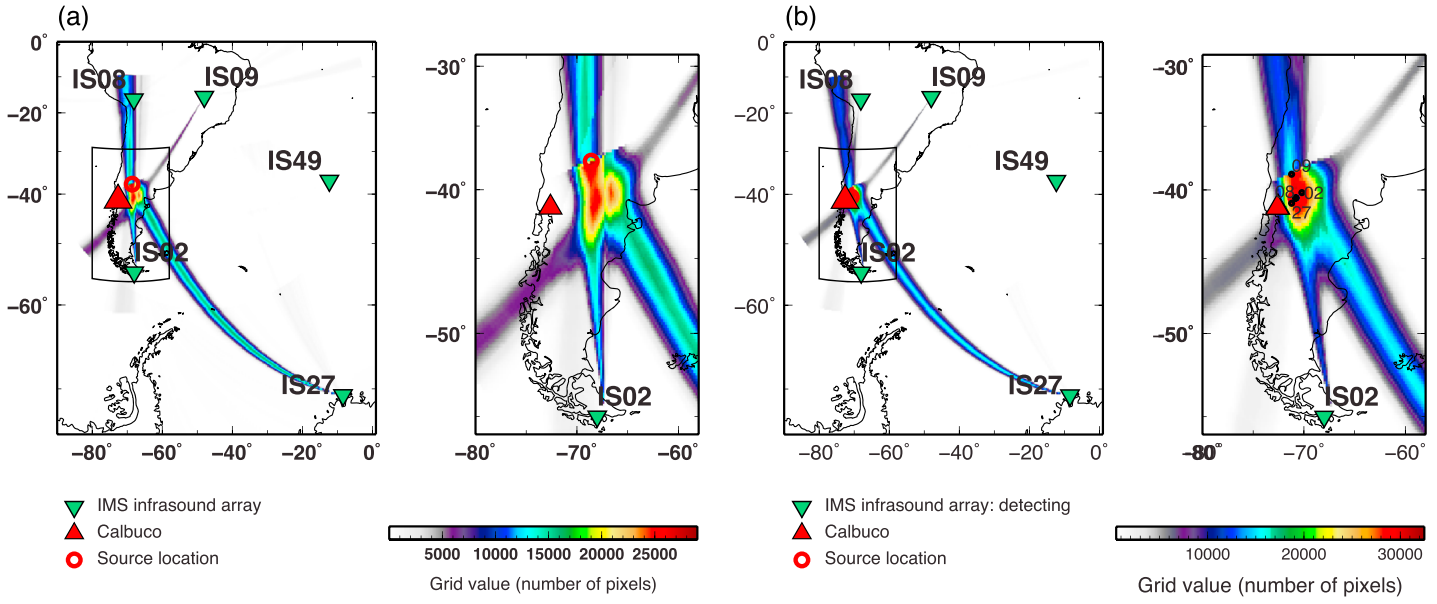

Figure 7. Automated source location 22–23 April 2015 from the five detecting IMS stations using the brute-force, grid-search, cross-bearings method of Matoza et al. (2017). (a) Without azimuth deviation correction (source location 522 km from true Calbuco location) and (b) with azimuth deviation correction using 3-D ray tracing and ECMWF (source location 172 km from true). The apparent discontinuity in the source image to the north results from the IS27 contribution and maximum distance parameter of 5,000 km. The large red circle is the source location solution (grid maximum). In Figure 7b, the small blue circle is the source location derived without using a maximum distance cutoff (coincident with red circle). The small black circles are the source locations from jackknife tests (e.g., label "27" corresponds to the location derived when station IS27 is not used). The jackknife solutions for IS08 and IS49 are coincident with the main source location (red and blue circles). An animation of the grid construction is shown in supporting information Movie S1. IMS = International Monitoring System; ECMWF = European Centre for Medium-Range Weather Forecasting.

Although ray tracing provides a prediction of azimuth deviations, in practice, explaining infrasound observations with currently available atmospheric specifications requires interactive manual analysis (e.g., Matoza, Le Pichon, et al., 2011). In particular, identifying eigenrays between the source and receiver is nontrivial, and propagation paths can be strongly dependent on stochastic small-scale perturbations to the available atmospheric profiles, often interpreted as gravity waves not captured in spatially smoothed atmospheric specifications (Assink et al., 2014; Green et al., 2011; Le Pichon et al., 2015; Smets et al., 2016). Our emphasis is on developing methods that could be applied rapidly to produce analysis products to aid volcano monitoring, or that could be applied automatically to large data archives; thus, we choose a more robust and simple approach.

We assume a source at Calbuco (source altitude fixed to 3 km) and launch rays at 5 azimuth values toward each station (from −5° to +5° of the great-circle azimuth in increments of 2.5°). For each azimuth, we launch 80 rays, with the elevation angles ranging from 0 to 40° in increments of 0.5° (sampling is done in elevation angle, not ray parameter). Among the 400 rays launched, those with stratospheric trajectories (defined as having a maximum turning height between 30 km and 60 km altitude) intercepting a box centered on the station of dimension 50 km × 50 km × 5 km (in longitude, latitude, elevation, respectively) are identified as a candidate. We define the final azimuth deviation values as the median of all candidates to represent averages over multiple propagation paths. We note that the observed and modeled azimuth deviations are up to 11° and 7°, respectively. Such large values can be expected for nearly southward propagation under a stratospheric wind jet (e.g., Le Pichon et al., 2005).

A natural extension of the method would be to include a crosswind correction in all look directions computed from each receiver to every trial source node based on the current atmospheric specification. We do not attempt that here, but our approach provides a preliminary indication of the importance of incorporating more realistic propagation corrections. Without the crosswind correction, the derived source location is 522 km from true (Figure 7a); with the correction, we obtain a source location at 172 km from true (Figure 7b). Thus, as expected, the crosswind correction significantly aids with signal association and attributing a detected event to a volcano.

We perform jackknife tests to investigate the contribution of individual stations to the source location solution (Figure 7b). For example, the location labeled "27" in Figure 7b corresponds to the source location derived without IS27 and using only the other four IMS stations (IS02, IS08, IS09, and IS49). In most cases (IS02, IS08, IS27, and IS49), the removal of one station has only a minor effect on the source location. However, IS09 has a slightly more important contribution given the source-receiver geometries and azimuthal coverage. We use a maximum distance cutoff of 5,000 km for the grids shown in Figure 7; however, removal of the distance cutoff produces an identical source location (blue circle, Figure 7b), indicating that the source locations are primarily controlled by backazimuth intersection.

4. Discussion

The two main explosive phases of the April 2015 eruption of Calbuco are well recorded on regional seismic stations out to 216 km (Figure 1), on regional single-sensor infrasound stations from 216 km to 1,540 km (Figure 4) and on IMS infrasound arrays at distances from 1,525 km to 5,122 km (Figures 3 and 4). For a real-time monitoring scenario, this case study exemplifies how incorporating regional seismo-acoustic data would help to dramatically reduce latency for eruption detection and notification compared to using the IMS data alone. For a celerity of 0.3 km/s, propagation time to GO07 (216 km) is 12 min, whereas to IS02 (1,525 km) it is 84 min.

Overall, the signal timing and duration determined from the remote IMS infrasound stations is consistent with the explosion chronology determined by Van Eaton et al. (2016) and as recorded on the regional seismic and infrasound stations, building confidence that volcanic explosion chronologies can be accurately inferred from remote infrasound observations for events of this magnitude (Figure 3b) (e.g., Matoza, Le Pichon, et al., 2011). Furthermore, our results indicate that an eruption event of this size can be automatically detected and located using remote IMS infrasound data, with improvements to the source location achieved by accounting for stratospheric crosswinds (section 3). The remaining source mislocation (172 km) is most likely a result of inaccuracies in the atmospheric specifications, leading to errors in simulated raypaths. For example, stratospheric wind speeds are often underestimated in atmospheric specifications (Le Pichon et al., 2005, 2015).

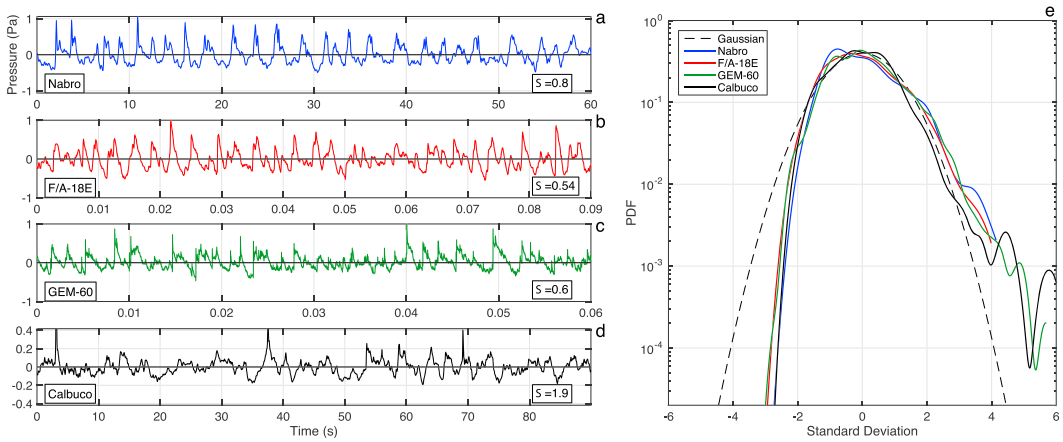

Figure 8. Comparison of the waveform skewness of Calbuco GO07 infrasound data (d) with infrasound data from (a) Nabro, and acoustic data from (b) an F/A-18E Super Hornet jet engine and (c) a GEM-60 solid rocket motor (Fee et al., 2013). The Nabro (IS19) and Calbuco (GO07) waveforms are filtered in the same band: 0.1–8 Hz. The Nabro and Calbuco plot origin times are 05:00:00 13 June 2011 and 05:04:00 23 April 2015, respectively. This figure is a reproduction of Figure 3 of Fee et al. (2013) with the Calbuco data added for comparison. (e) Probability density functions of the waveform amplitude, with all waveforms having similar skewed distributions with long positive tails. A Gaussian probability density function is shown in black for comparison. Note that the timescales of the volcano waveforms (Figures 8a and 8d) are ~300–1,000 times longer than the F/A-18E and GEM-60 signals (Figures 8b and 8c) as shown, consistent with similar jet-noise processes operating at larger spatial scales and correspondingly lower (infrasonic) frequencies (Fee et al., 2013; Matoza et al., 2009).

In addition, neglecting submesoscale variations in atmospheric specifications, including gravity waves, may lead to errors in predicted paths. In the case of a marginal duct, small perturbations to the atmospheric profile (e.g., gravity wave induced horizontal wind fluctuations) may be required to enable ducting (e.g., Green et al., 2011). Thus, gravity waves may establish a separate duct, with a different azimuth deviation prediction than that obtained without the gravity waves. The direct effect of gravity wave perturbations on along-path azimuth deviations is not yet understood but could be small if random wind direction perturbations average out along the propagation path. Uncertainties in backazimuth estimation using infrasound arrays provide additional error (Szuberla & Olson, 2004), which is approximated in our approach with the ±2° azimuth deviation tolerance used for the combined association and location (Matoza et al., 2017).

For a real-time detection scenario, the source location error of 172 km is not sufficient to identify a specific volcano and may lead to ambiguity as to which particular volcano erupted. However, for a remote volcano not monitored with local instrumentation, a source location with error of ~200 km could still be useful to trigger a search of satellite or other data. Completing the IMS network (e.g., planned station IS01, Bariloche, Argentina) and adding more regional infrasound arrays would both improve the location accuracy.

The seismo-acoustic cross-correlation and coherence analysis and observed polarization change above 2 Hz for the seismic data indicate that air-ground coupling is a significant component of the seismic eruption tremor waveforms at regional distances (Figures 5 and 6). Thus, existing seismic networks can help improve the infrasonic network detection capability (e.g., Cochran & Shearer, 2006; Fee et al., 2016; Hedlin et al., 2012).

We further investigate atmospheric influence on the propagation and detectability of the Calbuco eruption by modeling transmission loss (TL) from Calbuco using a frequency-dependent, semiempirical attenuation relationship derived from parabolic equation simulations (Figure 2) (Le Pichon et al., 2012; Tailpied et al., 2016). We chose this approach as it is fast to implement, requires relatively few model parameters, and is thus suitable as a near-real-time analysis tool. A rapid and simple model of infrasound propagation conditions would help volcano observatories to interpret observed signal detection for a given eruption, network geometry, and current atmospheric state. The attenuation relation accounts for the effects of source frequency, geometrical spreading, and absorption. The temporal and spatial variability of the atmosphere is described using the ECMWF operational high-spatial resolution forecasts. Along-path stratospheric wind averaged between altitudes 40 and 60 km is the primary atmospheric parameter in the empirical relation (Le Pichon et al., 2012).

The color scale in Figure 2 shows infrasound TL at 0.5 Hz from Calbuco at the ground surface; this frequency approximately corresponds to the highest observed signal-to-noise ratio for the Calbuco signals at the IMS infrasound stations. This map provides a prediction of the IMS network detection capability for this event

given the atmospheric specification. Overall, the geographic distribution of detecting stations is well explained to first order, which predicts <70 dB TL at detecting IMS stations (Figure 2). At the time of the eruption, steady stratospheric currents favor long-range propagation eastward. The observed celerity of 0.3 km/s is also consistent with stratospheric ducting (e.g., Brown et al., 2002). The lack of detection at IS14 is explained by the combined effects of signal attenuation and high background noise and clutter on oceanic islands (Brown et al., 2014; Matoza et al., 2013).

Recorded infrasound waveforms represent a convolution of the source-time function and the Green's function describing propagation from source to receiver. At regional to remote distances, propagation effects on recorded waveforms are significant and it is challenging to relate waveform features uniquely to source effects. The infrasound waveforms at station GO07 (216 km) during the first ~1.5–2 h of Phase 2 (~04:00–06:00 23 April 2015) exhibit repeated asymmetric, shock-like pressure pulses with positive waveform skewness, similar to those associated with the "crackle" phenomenon in audible noise from supersonic, heated jet, and rocket engines (Gee et al., 2007, 2009) (Figures 1 and 8). Asymmetric waveforms similar to those associated with crackle have been recorded associated with turbulent jetting at other volcanoes (e.g., Fee et al., 2013; Goto et al., 2014). Asymmetric infrasound waveforms are also associated with "chugging" (Lees et al., 2004), although chugging has a different spectral signature to that associated with turbulent jetting (e.g., Fee et al., 2013). The waveform shape and skewness of infrasound between ~04:00 and 6:00 23 April 2015 resemble that associated with crackle from supersonic jet and rocket engines, as well as the infrasound from the 2013 eruption of Nabro Volcano, Eritrea (Figure 8) (Fee et al., 2013).

The asymmetric GO07 waveforms may result from source effects, propagation effects (Lonzaga et al., 2015), or a combination of both. Nonlinear reshocking can occur for both thermospheric and stratospheric propagation, but is more severe for thermospheric paths (Lonzaga et al., 2015). To investigate propagation effects, full-waveform, broadband, and nonlinear numerical propagation modeling is required (e.g., de Groot-Hedlin, 2016; Lonzaga et al., 2015) but is beyond the scope of the present study. For the 2011 Nabro eruption, ray tracing and high trace-velocity estimates indicated a thermospheric path from the source to the receiver at 264 km range (Fee et al., 2013). For the 2015 Calbuco eruption, WASP-3D ray tracing using ECMWF fails to predict any arrivals at GO07 (216 km), likely because the atmospheric specifications are spatially smoothed. Nonlinear and broadband propagation effects can also explain infrasound observations in ray shadow zones in some cases (de Groot-Hedlin, 2016). The range of 216 km is short, but not unprecedented, for thermospheric arrivals; thermospheric arrivals at ~200 km have previously been observed (Gibbons et al., 2015; Reed, 1969; Whitaker & Mutschlecner, 2008).

The celerity estimates for arrivals at GO07 (0.3 km/s) are consistent with stratospheric propagation when using the explosion origin times of Van Eaton et al. (2016) or when fitting a constant celerity model to all recording infrasound stations (Figure 4 and Tables 1a and 1b). However, due to the emergent onsets of the signals, lack of local infrasound data, variations in signal-to-noise ratio across the network, and uncertainties in the derived explosion origin times, it is difficult to conclude with confidence that the GO07 observations are stratospheric arrivals based on available celerity information. Furthermore, for a long-duration, sustained eruption signal, the first-arrival celerity is not a robust indicator of the propagation path for the full waveform (Matoza, Le Pichon, et al., 2011). Steady transitions in trace velocity, dominant frequency, and backazimuth deviation have been observed in sustained eruption signals at arrays at remote distances, indicating a gradual transition from dominantly tropospheric, through dominantly stratospheric, to dominantly thermospheric trajectories in a continuous waveform (Matoza, Le Pichon, et al., 2011).

The observed GO07 infrasound waveform skewness is a broadband feature; a band-pass filter results in a waveform that is significantly less skewed (e.g., 0.5–9 Hz filter used in Figure 3). However, for the GO07 signals, low-frequency components (<0.5 Hz) are more important than high frequencies (>5 Hz) in forming the asymmetric waveforms. Applying a high-pass filter (>1 Hz) removes the waveform skewness. Applying a low-pass filter (<5 Hz) preserves the waveform skewness. That said, Figure 6 shows significant signal power at frequencies extending to the Nyquist frequency near ~18 Hz for the GO07 waveforms. These high-frequency signal components at a range of 216 km suggest propagation along a low attenuation path (turning below the thermosphere), and they could be produced at the source or by reshocking at altitude; numerical propagation modeling would be required to confirm the propagation path and the likely generation mechanism.

However, it remains possible that the wavefield is a superposition of phases including thermospheric phases; thus, the presence of high frequencies does not rule out that the asymmetry (which is dominant at lower frequencies) is a thermospheric effect. Waveform skewness is not observed at the IMS stations, which we interpret as due to attenuation of high frequencies at the greater ranges (>1,525 km) as well as lower signal-to-noise ratios at low frequencies (<0.5 Hz).

Although the cause of positive waveform skewness at volcanoes is currently unclear, it is possible that these observations are explained by supersonic flow during the beginning of Phase 2 and possibly a more gas-rich eruption column (Fee et al., 2013). The skewed infrasound waveforms also correspond temporally to the deposition of low-density pumice (Deposit C in Romero et al., 2016) and end approximately when the PDCs begin (Van Eaton et al., 2016). After this portion, the tephra consists of higher-density pumice (Deposit D) (Romero et al., 2016). These observations suggest a significant change in the plume density and dynamics at around 06:30 23 April 2015.

5. Conclusions

The two major explosive phases of the 22–23 April 2015 eruption of Calbuco volcano, Chile, were recorded on seismo-acoustic stations out to 1,540 km and on five stations of the IMS infrasound network out to 5,122 km. The remote IMS infrasound arrays provide an accurate explosion chronology consistent with the regional and local seismo-acoustic data, increasing confidence in the use of remote infrasound observations for automated detection, location, and characterization of explosive volcanism. Augmenting the IMS in regions of dense volcanism, even with relatively sparse regional seismo-acoustic networks, will dramatically enhance volcanic signal detection, reduce latency, and improve discrimination capability.

Acknowledgments
We used data from seismic network codes C (Chilean National Seismic Network), C1 (Red Sismologica Nacional), and GT (Global Telemetered Seismograph Network), downloaded from the IRIS DMC (http://www.iris.edu). Data from the CTBT IMS infrasound network are available through the CTBTO vDEC platform (https://www.ctbto.org/specials/vdec/). Our analysis included the use of ObsPy (Beyreuther et al., 2010) and PMCC (Le Pichon et al., 2010), and we used GMT for plotting (Wessel & Smith, 1991). We thank Danny Bowman, Weston Thelen, and an anonymous reviewer for their comments that helped to improve the manuscript. This work was supported by NSF grants EAR–1614855 and EAR-1614323.

References

Assink, J. D., Le Pichon, A., Blanc, E., Kallel, M., & Khemiri, L. (2014). Evaluation of wind and temperature profiles from ECMWF analysis on two hemispheres using volcanic infrasound. *Journal of Geophysical Research: Atmospheres*, *119*, 8659–8683. https://doi.org/10.1002/2014JD021632

Beyreuther, M., Barsch, R., Krischer, L., Megies, T., Behr, Y., & Wassermann, J. (2010). ObsPy: A Python toolbox for seismology. *Seismological Research Letters*, *81*(3), 530–533. https://doi.org/10.1785/gssrl.81.3.530

Brown, D., Ceranna, L., Prior, M., Mialle, P., & Le Bras, R. J. (2014). The IDC seismic, hydroacoustic and infrasound global low and high noise models. *Pure and Applied Geophysics*, *171*(3–5), 361–375. https://doi.org/10.1007/s00024-012-0573-6

Brown, D. J., Katz, C. N., Le Bras, R., Flanagan, M. P., Wang, J., & Gault, A. K. (2002). Infrasonic signal detection and source location at the Prototype International Data Centre. *Pure and Applied Geophysics*, *159*(5), 1081–1125. https://doi.org/10.1007/s00024-002-8674-2

Castruccio, A., Clavero, J., Segura, A., Samaniego, P., Roche, O., Le Pennec, J.-L., & Droguett, B. (2016). Eruptive parameters and dynamics of the April 2015 sub-Plinian eruptions of Calbuco volcano (southern Chile). *Bulletin of Volcanology*, *78*(9), 62. https://doi.org/10.1007/s00445-016-1058-8

Caudron, C., Taisne, B., Garces, M., Le Pichon, A., & Mialle, P. (2015). On the use of remote infrasound and seismic stations to constrain the eruptive sequence and intensity for the 2014 Kelud eruption. *Geophysical Research Letters*, *42*, 6614–6621. https://doi.org/10.1002/2015GL064885

Christie, D., & Campus, P. (2010). The IMS infrasound network: Design and establishment of infrasound stations. In A. L. Pichon, E. Blanc, & A. Hauchecorne (Eds.), *Infrasound monitoring for atmospheric studies* (Chapter 2, pp. 29–75). Netherlands: Springer. https://doi.org/10.1007/978-1-4020-9508-5_2

Cochran, E. S., & Shearer, P. M. (2006). Infrasound events detected with the Southern California Seismic Network. *Geophysical Research Letters*, *33*, L19803. https://doi.org/10.1029/2006GL026951

Dabrowa, A. L., Green, D. N., Rust, A. C., & Phillips, J. C. (2011). A global study of volcanic infrasound characteristics and the potential for long-range monitoring. *Earth and Planetary Science Letters*, *310*(3-4), 369–379. https://doi.org/10.1016/j.epsl.2011.08.027

De Angelis, S., Fee, D., Haney, M., & Schneider, D. (2012). Detecting hidden volcanic explosions from Mt. Cleveland Volcano, Alaska with infrasound and ground-coupled airwaves. *Geophysical Research Letters*, *39*, L21312. https://doi.org/10.1029/2012GL053635

de Groot-Hedlin, C. D. (2016). Long-range propagation of nonlinear infrasound waves through an absorbing atmosphere. *The Journal of the Acoustical Society of America*, *139*(4), 1565–1577. https://doi.org/10.1121/1.4944759

Dessa, J.-X., Virieux, J., & Lambotte, S. (2005). Infrasound modeling in a spherical heterogeneous atmosphere. *Geophysical Research Letters*, *32*, L12808. https://doi.org/10.1029/2005GL022867

Edwards, W. N., Eaton, D. W., McCausland, P. J., ReVelle, D. O., & Brown, P. G. (2007). Calibrating infrasonic to seismic coupling using the stardust sample return capsule shockwave: Implications for seismic observations of meteors. *Journal of Geophysical Research*, *112*, B10306. https://doi.org/10.1029/2006JB004621

Evers, L. G., & Haak, H. W. (2005). The detectability of infrasound in the Netherlands from the Italian volcano Mt. Etna. *Journal of Atmospheric and Solar - Terrestrial Physics*, *67*(3), 259–268. https://doi.org/10.1016/j.jastp.2004.09.002

Fee, D., Garces, M., & Steffke, A. (2010). Infrasound from Tungurahua Volcano 2006–2008: Strombolian to Plinian eruptive activity. *Journal of Volcanology and Geothermal Research*, *193*(1-2), 67–81. https://doi.org/10.1016/j.jvolgeores.2010.03.006

Fee, D., Haney, M., Matoza, R., Szuberla, C., Lyons, J., & Waythomas, C. (2016). Seismic envelope-based detection and location of ground-coupled airwaves from volcanoes in Alaska. *Bulletin of the Seismological Society of America*, *106*, 3. https://doi.org/10.1785/0120150244

Fee, D., & Matoza, R. S. (2013). An overview of volcano infrasound: from hawaiian to plinian, local to global. *Journal of Volcanology and Geothermal Research*, *249*, 123–139. https://doi.org/10.1016/j.jvolgeores.2012.09.002

Fee, D., Matoza, R. S., Gee, K. L., Neilsen, T. B., & Ogden, D. E. (2013). Infrasonic crackle and supersonic jet noise from the eruption of Nabro Volcano, Eritrea. *Geophysical Research Letters*, *40*, 4199–4203. https://doi.org/10.1002/grl.50827

Fee, D., Steffke, A., & Garces, M. (2010). Characterization of the 2008 Kasatochi and Okmok eruptions using remote infrasound arrays. *Journal of Geophysical Research*, *115*, DO0L10. https://doi.org/10.1029/2009JD013621

Garces, M., Fee, D., McCormack, D., Servranckx, R., Bass, H., Hetzer, C., et al. (2008). Prototype ASHE volcano monitoring system captures the acoustic fingerprint of stratospheric ash injection. *Eos, Transactions, American Geophysical Union*, *89*(40), 377–379.

Garcés, M., Hetzer, C., Merrifield, M., Willis, M., & Aucan, J. (2003). Observations of surf infrasound in Hawai'i. *Geophysical Research Letters*, *30*(24), 2264. https://doi.org/10.1029/2003GL018614

Gee, K. L., Giraud, J. H., Blotter, J. D., & Sommerfeldt, S. D. (2009). Energy based acoustical measurements of rocket noise, 15th AIAA/CEAS Aeroacoustics Conference (30th AIAA Aeroacoustics Conference). https://doi.org/10.2514/6.2009-3165

Gee, K. L., Sparrow, V. W., Atchley, A., & Gabrielson, T. B. (2007). On the perception of crackle in high-amplitude jet noise. *AIAA Journal*, *45*(3), 593–598. https://doi.org/10.2514/1.26484

Gibbons, S. J., Asming, V., Eliasson, L., Fedorov, A., Fyen, J., Kero, J., et al. (2015). The European Arctic: A laboratory for seismoacoustic studies. *Seismological Research Letters*, *86*(3), 917–928. https://doi.org/10.1785/0220140230

Global Volcanism Program (2013). *Volcanoes of the World v. 4.5.3*. In E. Venzke (Ed.). Washington, DC: Smithsonian Institution. Retrieved from https://doi.org/10.5479/si.GVP.VOTW4-2013, accessed on June 2016

Goto, A., Ripepe, M., & Lacanna, G. (2014). Wideband acoustic records of explosive volcanic eruptions at Stromboli: New insights on the explosive process and the acoustic source. *Geophysical Research Letters*, *41*, 3851–3857. https://doi.org/10.1002/2014GL060143

Green, D. N., Evers, L. G., Fee, D., Matoza, R. S., Snellen, M., Smets, P., & Simons, D. (2013). Hydroacoustic, infrasonic and seismic monitoring of the submarine eruptive activity and sub-aerial plume generation at south Sarigan, May 2010. *Journal of Volcanology and Geothermal Research*, *257*, 31–43. https://doi.org/10.1016/j.jvolgeores.2013.03.006

Green, D. N., Vergoz, J., Gibson, R., Le Pichon, A., & Ceranna, L. (2011). Infrasound radiated by the Gerdec and Chelopechene explosions: Propagation along unexpected paths. *Geophysical Journal International*, *185*(2), 890–910. https://doi.org/10.1111/j.1365-246X.2011.04975.x

Hedlin, M. A. H., de Groot-Hedlin, C., & Drob, D. (2012). A study of infrasound propagation using dense seismic network recordings of surface explosions. *Bulletin of the Seismological Society of America*, *102*(5), 1927–1937. https://doi.org/10.1785/0120110300

Ichihara, M., Takeo, M., Yokoo, A., Oikawa, J., & Ohminato, T. (2012). Monitoring volcanic activity using correlation patterns between infrasound and ground motion. *Geophysical Research Letters*, *39*, L04304. https://doi.org/10.1029/2011GL050542

IRIS DMC (2012). Data services products: Infrasound TA infrasound data products. http://doi:10.17611/DP/IS.1; http://ds.iris.edu/ds/products/infrasound/event/taired

Kamo, K., Ishihara, K., & Tahira, M. (1994). Infrasonic and seismic detection of explosive eruptions at Sakurajima volcano, Japan, and the PEGASAS-VE early-warning system. In T. C. Casadevall (Ed.), *Proceedings of the First International Symposium on Volcanic Ash and Aviation Safety* (Vol. 2047, pp. 357–365). U.S. Geol. Surv. Bull.

Le Pichon, A., Assink, J. D., Heinrich, P., Blanc, E., Charlton-Perez, A., Lee, C. F., et al. (2015). Comparison of co-located independent ground-based middle atmospheric wind and temperature measurements with numerical weather prediction models. *Journal of Geophysical Research: Atmospheres*, *120*, 8318–8331. https://doi.org/10.1002/2015JD023273

Le Pichon, A., Blanc, E., Drob, D., Lambotte, S., Dessa, J. X., Lardy, M., et al. (2005). Infrasound monitoring of volcanoes to probe high-altitude winds. *Journal of Geophysical Research*, *110*, D13106. https://doi.org/10.1029/2004JD005587

Le Pichon, A., Ceranna, L., & Vergoz, J. (2012). Incorporating numerical modeling into estimates of the detection capability of the IMS infrasound network. *Journal of Geophysical Research*, *117*, D05121. https://doi.org/10.1029/2011JD016670

Le Pichon, A., Matoza, R., Brachet, N., & Cansi, Y. (2010). Recent enhancements of the PMCC infrasound signal detector, Inframatics, September 2010 issue

Le Pichon, A., Maurer, V., Raymond, D., & Hyvernaud, O. (2004). Infrasound from ocean waves observed in Tahiti. *Geophysical Research Letters*, *31*, L19103. https://doi.org/10.1029/2004GL020676

Le Pichon, A., Vergoz, J., Blanc, E., Guilbert, J., Ceranna, L., Evers, L., & Brachet, N. (2009). Assessing the performance of the International Monitoring System's infrasound network: Geographical coverage and temporal variabilities. *Journal of Geophysical Research*, *114*, D08112. https://doi.org/10.1029/2008JD010907

Lees, J. M., Gordeev, E. I., & Ripepe, M. (2004). Explosions and periodic tremor at Karymsky volcano, Kamchatka, Russia. *Geophysical Journal International*, *158*(3), 1151–1167. https://doi.org/10.1111/j.1365-246X.2004.02239.x

Lonzaga, J. B., Waxler, R. M., Assink, J. D., & Talmadge, C. L. (2015). Modelling waveforms of infrasound arrivals from impulsive sources using weakly non-linear ray theory. *Geophysical Journal International*, *200*(3), 1347–1361. https://doi.org/10.1093/gji/ggu479

Matoza, R. S., & Fee, D. (2014). Infrasonic component of volcano-seismic eruption tremor. *Geophysical Research Letters*, *41*, 1964–1970. https://doi.org/10.1002/2014GL059301

Matoza, R. S., Fee, D., Garces, M. A., Seiner, J. M., Ramon, P. A., & Hedlin, M. A. H. (2009). Infrasonic jet noise from volcanic eruptions. *Geophysical Research Letters*, *36*, L08303. https://doi.org/10.1029/2008GL036486

Matoza, R. S., Green, D. N., Le Pichon, A., Shearer, P. M., Fee, D., Mialle, P., & Ceranna, L. (2017). Automated detection and cataloging of global explosive volcanism using the International Monitoring System infrasound network. *Journal of Geophysical Research: Solid Earth*, *122*, 2946–2971. https://doi.org/10.1002/2016JB013356

Matoza, R. S., Hedlin, M. A. H., & Garces, M. A. (2007). An infrasound array study of Mount St. Helens. *Journal of Volcanology and Geothermal Research*, *160*, 249–262. https://doi.org/10.1016/j.jvolgeores.2006.10.006

Matoza, R. S., Landès, M., Le Pichon, A., Ceranna, L., & Brown, D. (2013). Coherent ambient infrasound recorded by the International Monitoring System. *Geophysical Research Letters*, *40*, 429–433. https://doi.org/10.1029/2012GL054329

Matoza, R. S., Le Pichon, A., Vergoz, J., Herry, P., Lalande, J.-M., Lee, H., et al. (2011). Infrasonic observations of the June 2009 Sarychev Peak eruption, Kuril Islands: Implications for infrasonic monitoring of remote explosive volcanism. *Journal of Volcanology and Geothermal Research*, *200*(1-2), 35–48. https://doi.org/10.1016/j.jvolgeores.2010.11.022

Matoza, R. S., Vergoz, J., Le Pichon, A., Ceranna, L., Green, D. N., Evers, L. G., et al. (2011). Long-range acoustic observations of the Eyjafjallajökull eruption, Iceland, April–May 2010. *Geophysical Research Letters*, *38*, L06308. https://doi.org/10.1029/2011GL047019

Mialle, N., Brachet, P., Gaillard, A., Le Pichon, E., Blanc, D., Tailpied, E., et al. (2015). Towards a volcanic notification system with infrasound data: Use of infrasound data in support of the VAACs in the framework of ARISE project, in World Meteorological Organization 7th International Workshop on Volcanic Ash (IWVA/7), Anchorage, Alaska.

Nippress, A., & Green, D. N. (2017). Sensitivity of the International Monitoring System infrasound network to elevated sources: A western Eurasia case study. *Geophysical Journal International*, *211*(2), 920–935. https://doi.org/10.1093/gji/ggx342

Reed, J. W. (1969). Climatology of airblast propagations from Nevada test site nuclear airbursts, Sandia Laboratories Report SC-RR-69-572. Albuquerque, NM. Retrieved from http://www.dtic.mil/dtic/

Romero, J. E., Morgavi, D., Arzilli, F., Daga, R., Caselli, A., Reckziegel, F., et al. (2016). Eruption dynamics of the 22–23 April 2015 Calbuco Volcano (Southern Chile): Analyses of tephra fall deposits. *Journal of Volcanology and Geothermal Research*, *317*, 15–29. https://doi.org/10.1016/j.jvolgeores.2016.02.027

Shults, K., Astafyeva, E., & Adourian, S. (2016). Ionospheric detection and localization of volcano eruptions on the example of the April 2015 Calbuco events. *Journal of Geophysical Research: Space Physics*, *121*, 10,303–10,315. https://doi.org/10.1002/2016JA023382

Smets, P. S. M., Assink, J. D., Le Pichon, A., & Evers, L. G. (2016). ECMWF SSW forecast evaluation using infrasound. *Journal of Geophysical Research: Atmospheres*, *121*, 4637–4650. https://doi.org/10.1002/2015JD024251

Strick, E., & Ginzbarg, A. S. (1956). Stoneley-wave velocities for a fluid-solid interface. *Bulletin of the Seismological Society of America*, *46*, 281–292.

Szuberla, C. A. L., & Olson, J. V. (2004). Uncertainties associated with parameter estimation in atmospheric infrasound arrays. *The Journal of the Acoustical Society of America*, *115*(1), 253–258. https://doi.org/10.1121/1.1635407

Tailpied, D., Le Pichon, A., Marchetti, E., Assink, J., & Vergniolle, S. (2016). Assessing and optimizing the performance of infrasound networks to monitor volcanic eruptions. *Geophysical Journal International*, *208*(1), 437–448. https://doi.org/10.1093/gji/ggw400

Ulivieri, G., Ripepe, M., & Marchetti, E. (2013). Infrasound reveals transition to oscillatory discharge regime during lava fountaining: Implication for early warning. *Geophysical Research Letters*, *40*, 3008–3013. https://doi.org/10.1002/grl.50592

Valderrama, O., Cardona, C., & Gil-Cruz, F. (2016). Subplinian eruption of Calbuco volcano (Chile), April 22th, an example of VEI-4 explosive eruption with few precursor signals, Paper Presented at Cities on Volcanoes 9, 20–25 November, Puerto Varas, Chile

Valderrama, O., Franco, L., & Gil-Cruz, F. (2015). Erupción intempestiva del volcán Calbuco, Abril 2015. Congreso Geológico Chileno, No. XIV, La Serena, Chile

Van Eaton, A. R., Amigo, Á., Bertin, D., Mastin, L. G., Giacosa, R. E., González, J., et al. (2016). Volcanic lightning and plume behavior reveal evolving hazards during the April 2015 eruption of Calbuco volcano, Chile. *Geophysical Research Letters*, *43*, 3563–3571. https://doi.org/10.1002/2016GL068076

Vidal, L., Nesbitt, S., Salio, P., Osores, S., Farias, C., Rodriguez, A., et al. (2015). *C-band dual-polarization observations of a massive volcanic eruption in South America*. Paper presented at 37th Conference on Radar Meteorology, Am. Meteorol. Soc., Norman, OK, 14–18 September.

Virieux, J., Garnier, N., Blanc, E., & Dessa, J. X. (2004). Paraxial ray tracing for atmospheric wave propagation. *Geophysical Research Letters*, *31*, L20106. https://doi.org/10.1029/2004GL020514

Walker K. T., & Hedlin, M. A. H. (2010). A review of wind-noise reduction methodologies. In A. L. Pichon, E. Blanc, & A. Hauchecorne (Eds.), *Infrasound monitoring for atmospheric studies* (Chapter 5, 141–182). Netherlands: Springer. https://doi.org/10.1007/978-1-4020-9508-5_5

Wessel, P., & Smith, W. H. F. (1991). Free software helps map and display data. *Eos, Transactions American Geophysical Union*, *72*(41), 441.

Whitaker, R. W., & Mutschlecner, J. P. (2008). A comparison of infrasound signals refracted from stratospheric and thermospheric altitudes. *Journal of Geophysical Research*, *113*, D08117. https://doi.org/10.1029/2007JD008852